

The Optical/Near-IR Colours of Red Quasars

Paul J. Francis,^{1,2} Matthew T. Whiting³ and Rachel L. Webster³

¹Research School of Astronomy and Astrophysics, Australian National University, Canberra, ACT 0200, Australia
pfrancis@mso.anu.edu.au

²Joint appointment with the Department of Physics and Theoretical Physics, Faculty of Science, Australian National University, Canberra, ACT 0200, Australia

³School of Physics, University of Melbourne, Parkville, Vic. 3052, Australia
mwhiting, rwebster@physics.unimelb.edu.au

Received 1999 July 5, accepted 2000 January 7

Abstract: We present quasi-simultaneous multi-colour optical/near-IR photometry for 157 radio selected quasars, forming an unbiased sub-sample of the Parkes Flat-Spectrum Sample. Data are also presented for 12 optically selected QSOs, drawn from the Large Bright QSO Survey. The spectral energy distributions of the radio- and optically-selected sources are quite different. The optically selected QSOs are all very similar: they have blue spectral energy distributions curving downwards at shorter wavelengths. Roughly 90% of the radio-selected quasars have roughly power-law spectral energy distributions, with slopes ranging from $F_\nu \propto \nu^0$ to $F_\nu \propto \nu^{-2}$. The remaining 10% have spectral energy distributions showing sharp peaks: these are radio galaxies and highly reddened quasars. Four radio sources were not detected down to magnitude limits of $H \sim 19.6$. These are probably high redshift ($z > 3$) galaxies or quasars. We show that the colours of our red quasars lie close to the stellar locus in the optical: they will be hard to identify in surveys such as the Sloan Digital Sky Survey. If near-IR photometry is added, however, the red power-law sources can be clearly separated from the stellar locus: IR surveys such as 2MASS should be capable of finding these sources on the basis of their excess flux in the K -band.

Keywords: quasars: general—methods: observational

1 Introduction

It was long believed that quasars are blue. The optical/near-IR colours of optically selected QSOs are indeed uniformly very blue (e.g. Neugebauer et al. 1987; Francis 1996). It was therefore a surprise when substantial numbers of extremely red quasars were identified in radio-selected samples (e.g. Rieke, Lebofsky & Wisniewski 1982; Ledden & O'Dell 1983; Webster et al. 1995; Stickel, Rieke & Kühr 1996). The biggest sample of these objects is that of Webster et al., who were studying a sample of radio-loud quasars with flat radio spectra: the Parkes Half-Jansky Flat-Spectrum survey, a complete sample of 323 sources with fluxes at 2.7 GHz ($S_{2.7}$) of greater than 0.5 Jy, and radio spectral indices α ($S_\nu \propto \nu^\alpha$) with $\alpha > -0.5$ as measured between 2.7 and 5.0 GHz (Drinkwater et al. 1997). While some of these Parkes sources had $B_J - K_n$ colours as blue as any optically selected QSOs, most had redder $B_J - K_n$ colours, and some were amongst the reddest objects on the sky.

Why should the Parkes sources be so red? A variety of theories were proposed:

- The B_J magnitudes of the Parkes sample were measured many years before the K_n magnitudes. Quasars with flat radio spectra are known to be highly variable: this could thus introduce a scatter into the $B_J - K_n$ colours, though it is hard to see why it should introduce a systematic reddening.
- Elliptical galaxies with redshifts $z > 0.1$ have very red $B_J - K_n$ colours, due to the redshifted 400 nm break. If the host galaxies make a significant contribution to the integrated light from the Parkes sources, this could produce the red colours. Masci, Webster & Francis (1998), however, used spectra to show that this effect was only significant for $\sim 10\%$ of the sample.
- The B_J magnitudes were derived from COSMOS scans of UK Schmidt plates, and are subject to substantial systematic errors, which could introduce scatter into the $B_J - K_n$ colours (O'Brian, Webster & Francis 2000, in preparation), though this too should not introduce a systematic reddening.

- Parkes quasars could have the same intrinsic colours as optically selected QSOs, but be reddened by dust somewhere along the line of sight (Webster et al. 1995).
- Flat-radio-spectrum quasars are thought to have relativistic jets: if the synchrotron emission from these jets has a very red spectrum and extended into the near-IR, it could account for the red colours (Serjeant & Rawlings 1996).

In this paper, we test the results of Webster et al. (1995) by obtaining much better photometry of a large sub-set of the Parkes sources. To minimise the effects of variability, all our photometry for a given source was obtained within a period of at most six days. All the data were obtained from photometrically calibrated images and, rather than relying on only two bands (B_J and K_n), we obtained photometry in every band from B to K_n .

In principle, multi-colour photometry should enable us to discriminate between the dust and synchrotron models. If quasars have intrinsically blue power-law continua (e.g. $F_\nu \propto \nu^{-0.3}$, Francis 1996), reddened by a foreground dust screen with an extinction $E(B-V)$ between the B and V bands (in magnitudes) and an optical depth inversely proportional to wavelength, then the observed continuum slope will be

$$F_\lambda \propto e^{-2E(B-V)/\lambda} \lambda^{-1.7}, \quad (1)$$

where λ is the wavelength in μm . This is plotted in Figure 1. Note the very characteristic ‘n’ shape, as the dust absorption increases exponentially into the blue.

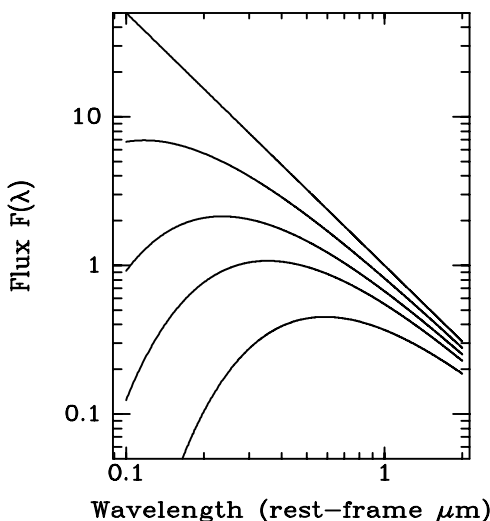


Figure 1—Continuum shapes of dust affected quasars. The extinction $E(B - V)$ increases downwards: values are 0, 0.1, 0.2, 0.3 and 0.4. Note the characteristic ‘n’ shape.

If, alternatively, the redness is caused by the addition of some red synchrotron emission component to the underlying blue continuum, continuum shapes

will have a characteristic ‘u’ shape, dominated by the underlying blue flux at short wavelengths but by the new synchrotron component at longer wavelengths (Figure 2).

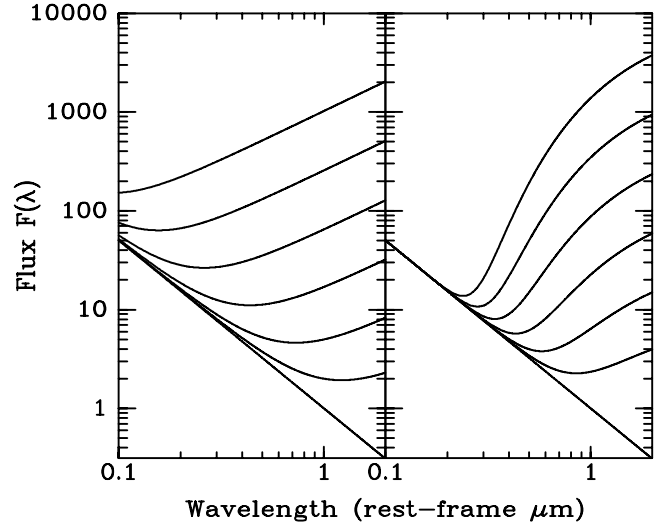


Figure 2—Continuum shapes of quasars with an additional red emission component. To show some of the possibilities, two different arbitrary functional forms have been chosen for the red component: a power-law (left) and an exponential (right). The strength of this red component increases upwards. Note the characteristic ‘u’ shape. The plausibility of synchrotron models is discussed in Whiting, Webster & Francis (2000).

Table 1. Observing log

Night code	Date	Telescope/Instrument
A	April 12, 1997	1m
B	April 13, 1997	1m
C	April 14, 1997	2.3m Imager
D	April 15, 1997	2.3m Imager
E	April 16, 1997	2.3m Caspir
F	April 17, 1997	2.3m Caspir
I	July 12, 1997	1m
J	July 13, 1997	1m
K	July 14, 1997	1m
L	July 13, 1997	2.3m Imager
M	July 14, 1997	2.3m Imager
N	July 15, 1997	2.3m Caspir
O	July 16, 1997	2.3m Caspir
P	July 17, 1997	2.3m Caspir
Q	July 18, 1997	2.3m Caspir
R	July 19, 1997	2.3m Caspir
S	July 20, 1997	2.3m Caspir
T	Sept 7, 1997	1m
U	Sept 8, 1997	1m
V	Sept 9, 1997	2.3m Imager
W	Sept 10, 1997	2.3m Imager
X	Sept 11, 1997	2.3m Caspir
Y	Sept 12, 1997	2.3m Caspir
Z	Sept 13, 1997	2.3m Caspir

If radio-quiet red quasars exist, they cannot be selected by conventional optical surveys. We show that by combining optical and near-IR data, it should be possible to select any radio-quiet sources with the colours of most of our radio-selected red quasars.

Table 2. (Continued)

Name	Redshift <i>z</i>	Morpho- logy	<i>B</i>	<i>V</i>	<i>R</i>	<i>I</i>	<i>J</i>	<i>H</i>	<i>K_n</i>
Letters indicate observation dates, numbers are exposure times (seconds)									
PKS 1616+063	2.088	point	J	300	J	300	J	300	O
PKS 1635-035	2.856	point	D	600	D	600	D	600	F
PKS 1648+015	...	faint	C	600	C	600	C	600	E
PKS 1649-062	...	faint	C	3000	C	2400
PKS 1654-020	2.000	faint	M	1800	M	1800	M	1800	Q
PKS 1655+077	0.621	point	V	600	V	600	V	300	Y
PKS 1656+053	0.887	point	I	300	I	300	I	300	P
PKS 1705+018	2.576	point	I	300	I	300	I	300	Q
PKS 1706+006	0.449	faint	V	1200	V	600	V	300	X
PKS 1725+044	0.296	point	A	600	A	300	A	300	E
PKS 1732+094	...	faint	M	1800	L	1200	L	1200	P
PKS 1933-400	0.965	point	A	300	A	300	A	300	F
PKS 1953-325	1.242	point	I	300	I	300	I	300	N
PKS 1954-388	0.626	point	I	300	I	300	I	300	N
PKS 1958-179	0.652	point	I	300	I	300	I	300	N
PKS 2000-330	3.783	point	I	300	I	300	I	300	P
PKS 2002-185	0.859	point	B	600	B	300	B	300	F
PKS 2004-447	0.240	point	A	300	A	300	A	300	F
PKS 2008-159	1.178	point	I	300	I	300	I	300	N
PKS 2021-330	1.471	point	J	300	I	300	I	300	NQ
PKS 2022-077	1.388	point	J	600	J	600	J	600	N
PKS 2037-253	1.574	point	J	300	J	300	J	300	O
PKS 2044-168	1.937	point	J	300	J	300	J	300	N
PKS 2047+098	...	faint	VW	1800	W	4200
PKS 2053-044	1.177	point	J	300	J	300	J	300	O
PKS 2056-369	...	faint	M	2400	L	1800	O
PKS 2058-135	0.029	galaxy ⁱ	J	120	J	30	J	30	Q
PKS 2058-297	1.492	point	J	300	J	300	J	300	P
PKS 2059+034	1.012	point	J	300	J	300	J	300	Q
PKS 2106-413	1.055	point	J	300	J	300	J	300	Q
PKS 2120+099	0.932	point	T	300	T	300	T	300	X
PKS 2121+053	1.941	point	J	300	J	300	J	300	Q
PKS 2126-158	3.266	point	L	600	L	1860	L	1860	P
PKS 2127-096	0.780	faint	T	600	T	300	T	300	X
PKS 2128-123	0.499	point	K	300	K	300	K	300	O
PKS 2131-021	1.285	point	K	900	K	300	K	300	Q
PKS 2134+004	1.937	point	K	300	K	300	K	300	Q
PKS 2135-248	0.821	point	K	300	K	300	K	300	Q
PKS 2140-048	0.344	point	K	300	K	300	K	300	Q
PKS 2143-156	0.698	point	K	300	K	300	K	300	Q
PKS 2144+092	1.113	point	T	300	T	300	T	300	X
PKS 2145-176	2.130	point	T	300	T	300	T	300	X
PKS 2145+067	0.999	point	V	120	V	120	V	120	U
PKS 2149-307	2.345	point	T	300	T	300	T	300	X
PKS 2149+056	0.740	faint	M	1800	M	1800	M	1200	Q
PKS 2149+069	1.364	point	V	120	V	120	V	120	X
PKS 2155-152	0.672	point	M	1200	M	1200	M	1800	Q
PKS 2200-238	2.120	point	T	300	T	300	T	300	Y
PKS 2203-188	0.619	point	T	300	T	300	T	300	Y
PKS 2206-237	0.086	galaxy ^j	V	120	V	120	V	120	Y
PKS 2208-137	0.392	point	V	120	V	120	V	120	Y
PKS 2210-257	1.833	point	V	120	V	120	V	120	Y
PKS 2212-299	2.703	point	V	120	V	120	V	120	Y
PKS 2215+020	3.572	point	V	600	V	600	V	300	Y
PKS 2216-038	0.901	point	L	600	L	600	L	1860	P
PKS 2223-052	1.404	point	V	120	V	120	V	120	Z
PKS 2227-088	1.561	point	V	120	V	120	V	120	Z
PKS 2227-399	0.323	point	V	120	V	120	V	120	Z
PKS 2229-172	1.780	faint	V	600	V	600	V	300	Z
PKS 2233-148	0.609	point	V	600	V	300	V	300	Z
PKS 2239+096	1.707	point	W	300	W	300	W	300	Z
PKS 2240-260	0.774	point	W	180	W	180	W	180	Z
PKS 2243-123	0.630	point	W	180	W	180	W	180	Z
PKS 2245-328	2.268	point	W	180	W	180	W	180	Z
PKS 2245+029	...	point	W	1200	W	600	W	600	X
PKS 2252-090	...	faint	W	1800	W	1800	W	600	X
PKS 2312-319	1.323	point	J	300	J	300	J	300	O
PKS 2313-438	1.847	point	J	300	J	300	J	300	Q
PKS 2314-409	2.448	point	J	300	J	300	J	300	Q
PKS 2329-415	0.671	point	J	300	J	300	J	300	Q
PKS 2337-334	...	faint	L	600	L	600	L	1200	O
PKS 2344-192	...	faint	L M	1800	...	L	600	L	600
PKS 2345-167	0.576	point	K	300	K	300	K	300	Q
PKS 2351-154	2.675	point	K	300	K	300	K	300	Q
PKS 2354-117	0.960	point	K	300	K	300	K	300	Q
L 2110-4509	0.555	point	U	300	U	300	U	300	Y
L 2111-4335	1.708	point	U	300	U	300	U	300	Y
L 2111-4506	1.376	point	U	300	U	300	U	300	Y
L 2113-4305	1.249	point	U	300	U	300	U	300	Y
L 2113-4345	2.053	point	U	300	U	300	U	300	Y
L 2113-4538	0.946	point	U	300	U	300	U	300	...
L 2114-4335	1.318	point	W	180	W	180	W	180	...

Table 2. (Continued)

Name	Redshift <i>z</i>	Morph- ology	<i>B</i>	<i>V</i>	<i>R</i>	<i>I</i>	<i>J</i>	<i>H</i>	<i>K_n</i>
L 2114-4346	2.041	point	W 180	W 180	W 180	W 180	0
L 2114-4501	0.597	point	W 180	W 180	W 180	W 180	0
L 2116-4439	1.480	point	W 180	W 180	W 180	W 180	0
L 2118-4702	1.332	point	W 180	W 180	W 180	W 180 Z	240
L 2119-4415	0.728	point	W 180	W 180	W 180	W 180	Z 240	Z 240	Z 240

^a Use circular photometric aperture of radius 45'' ^b Aperture radius 10'' ^c Aperture radius 8'' ^d Aperture radius 15'' ^e Aperture radius 8'' ^f Aperture radius 20'' ^g Aperture radius 35'' ^h Aperture radius 5'' ⁱ Aperture radius 10'' ^j Aperture radius 14''.

Table 3. Assumed fluxes of a zero magnitude star

Filter	Mean wavelength (μm)	Flux of zero magnitude star ($F_\lambda, \text{W m}^{-2} \text{nm}^{-1}$)
<i>B</i>	0.440	6.32×10^{-11}
<i>V</i>	0.550	3.64×10^{-11}
<i>R</i>	0.700	2.18×10^{-11}
<i>I</i>	0.880	1.13×10^{-11}
<i>J</i>	1.239	3.11×10^{-12}
<i>H</i>	1.649	1.15×10^{-12}
<i>K</i>	2.132	4.10×10^{-13}

This paper describes the observations, presents the data, includes some simple phenomenological analyses of the results, and discusses the colour selection of red quasars in the optical and near-IR. We defer the detailed modelling of the data to the companion paper by Whiting, Webster & Francis (2000).

2 Observations

We obtained quasi-simultaneous *B*, *V*, *R*, *I*, *J*, *H* and *K_n* photometry of a subset of the Parkes sample. Observations were taken during 26 nights in 1997 (Table 1) at Siding Spring Observatory. Optical images were obtained with either the 1 m telescope, or with the imager on the 2.3 m telescope. Near-IR images were obtained with the CASPIR 256×256 InSb array camera (McGregor et al. 1994) on the 2.3 m telescope. A total of 157 Parkes sources were observed in some or all of the bands, as well as a small control sample of 12 optically selected QSOs randomly selected from the Large Bright QSO survey (LBQS, Morris et al. 1991); an optical QSO survey well matched in size and redshift distribution to the Parkes sample. To minimise the effects of variability, all the observations of an individual source were made within, at most, a six-day period (Table 2). Flat spectrum quasars typically vary by 10% or less on these timescales, though very occasionally greater variations are seen, typically in BL Lac objects (e.g. Wagner et al. 1990; Heidt & Wagner 1996). Only data taken in photometric conditions were used: seeing was typically 1–2''.

Bright objects were typically observed for approximately five minutes in each band. Fainter objects were observed for up to two hours in our most sensitive bands (*R*, *I* and *H*). If they were seen in these bands, we observed them in progressively bluer bands as time allowed. Four sources

were not detected in any band: PKS 1535+004, PKS 1601–222, PKS 1649–062 and PKS 2047+098.

About five standard stars, spanning a range of colours, were observed each night: in the optical, the Graham E regions (Graham 1982) were used, while in the near-IR, photometric calibration was obtained using the IRIS standard stars, which have magnitudes on the Carter SAAO system (Carter & Meadows 1995). Within individual nights, the scatter in photometric zero points (without using colour corrections) was $\leq 3\%$ rms, so all the standards in a given band were simply averaged to give the final calibration.

All 98 Parkes sources lying in the R.A. ranges 00:36–00:57, 01:53–02:40 and 14:50–22:52 (B1950) were observed in both the optical and the IR: these should thus form an unbiased, complete subsample of the whole Parkes Half-Jansky sample. The remaining 59 sources were selected for observation mainly on the basis of prevailing weather conditions, and so should also form a reasonably unbiased subsample. No selection was made against radio galaxies: sources with resolved optical or near-IR images (as classified by the COSMOS plate measuring machine from UK Schmidt plates, and checked by visual inspection of our images) are listed in Table 2. Where appropriate, they are excluded from the following analysis.

Optical images were bias- and overscan-subtracted, and then flat fielded using twilight sky flats. For the fainter sources, multiply dithered 300- or 600-second exposures were taken: these were combined using inverse variance weighting. The infrared exposures were made up of multiple dithered 60 s images, each made up of two averaged 30 s exposures in *J*, six averaged 10 s exposures in *H* and twelve averaged 5 s exposures in *K_n*. These were bias- and dark-subtracted, and then corrected for the nonlinearity of the CASPIR detector using a simple quadratic correction term (derived from plots of median counts against exposure time obtained from dome flats). Known bad pixels were replaced by the interpolated flux from neighbouring pixels. Flat fields were obtained by taking exposures of the dome with lamps on and off, and subtracting one from the other: this removes the contribution from telescope emission, and substantially improves the photometric accuracy attainable. Individual images were sky subtracted, using a median of the 10

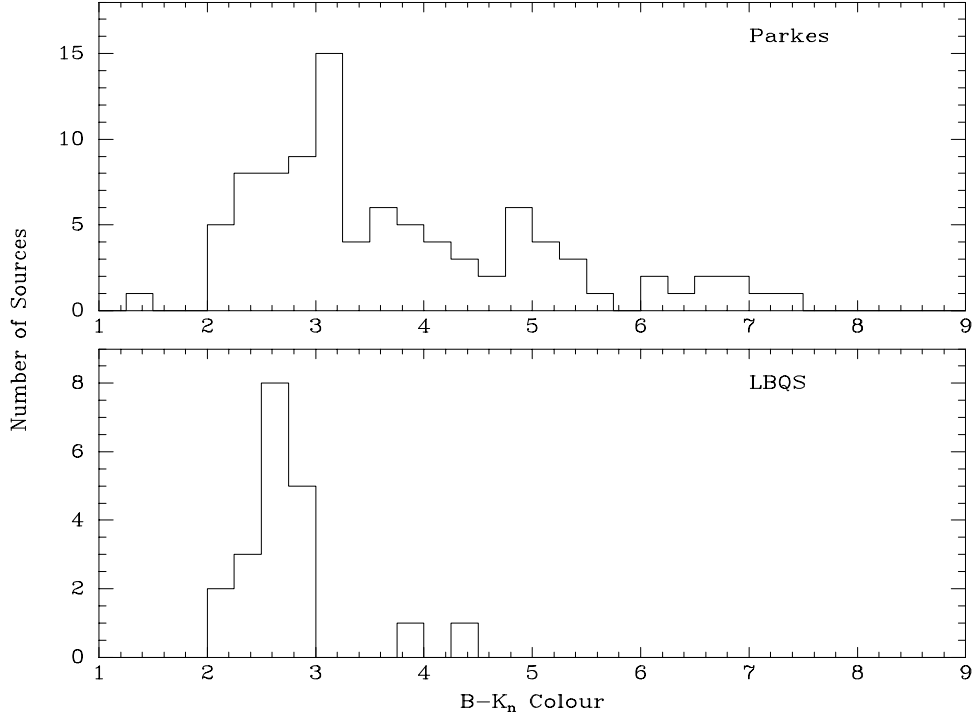


Figure 3—Distribution of $B - K_n$ colours for the Parkes sample (top), and the optically selected LBQS sample (bottom). Sources with spatially extended images (radio galaxies) have been excluded, as have sources with redshift $z > 3$ (as the Ly α forest depressed the B -band flux). Only Parkes sources within the complete sub-sample have been used. The LBQS data from this paper have been supplemented by data from Francis (1996).

images taken nearest in time. The dithered images were then aligned and combined, using the median to remove residual errors.

The radio sources were identified from the radio positions by using astrometry from nearby stars, bootstrapped from positions in the COSMOS/UKST and APM/POSS sky catalogues, maintained on-line at the Anglo-Australian Observatory. Magnitudes were then measured using circular apertures, with the sky level determined from the median flux in an annulus around the sky aperture. For unresolved sources, the photometric apertures were set by the seeing: typical aperture radii were $\sim 5''$. For resolved sources (mostly low redshift radio galaxies) larger circular apertures were used, centred on the galactic nucleus. These larger aperture radii are listed in the footnotes to Table 2. Standard stars were measured with similar aperture sizes.

Quoted errors are the sum (in quadrature) of random errors and an assumed 5% error in the photometric zero points. Random errors were determined by measuring the rms (root-mean-squared) pixel-to-pixel variation in sky regions, and scaling to the aperture size used. This will be accurate for fainter (sky or read-noise limited) sources, but will underestimate random errors for the brightest few sources. The photometric zero point errors were estimated from the scatter in zero points between different standard star measurements in an individual night: typical rms scatters are $\leq 3\%$,

so we adopted a conservative value of 5% as our zero point error.

For modelling and plotting purposes, we converted the magnitudes into fluxes. We assumed fluxes for zero magnitude objects as listed in Table 3. In the optical, our filter sets approximate the Johnson & Cousins system, and were calibrated using the Graham standards (also approximating Johnson & Cousins). The zero magnitude star fluxes for this system were taken from Bessell, Castelli & Plez (1998). In the infrared, our observations used the CASPIR filter set calibrated by the IRIS standards. Zero magnitude fluxes were calculated by P. McGregor, assuming that Vega is well represented in the near-IR by a black body of temperature 11200 K, and normalisation $F_\lambda(555 \text{ nm}) = 3.44 \times 10^{-12} \text{ W cm}^{-2} \mu\text{m}^{-1}$ (Bersanelli, Bouchet & Falomo 1991). These normalisations agree closely with those quoted for UKIRT near-IR standards (MacKenty et al. 1997). Our observations were made with the K_n filter, but were calibrated using the quoted K magnitudes of the IRIS standards without applying a colour correction term, and should thus be normalised to a K -band zero point.

3 Results and Discussion

3.1 The Colour Distribution

The results are listed in Table 4. Quoted errors are 1σ ; upper limits are 3σ .

Table 4. (Continued)

Name	<i>B</i>	<i>V</i>	<i>R</i>	<i>I</i>	<i>J</i>	<i>H</i>	<i>K_n</i>
L 2116-4439	18.61±0.06	18.20±0.06	17.80±0.05	17.40±0.06
L 2118-4702	19.21±0.08	18.98±0.07	18.64±0.06	18.40±0.08	16.67±0.30
L 2119-4415	18.02±0.05	17.72±0.05	17.43±0.05	16.88±0.05	16.07±0.06	15.68±0.06	15.03±0.09

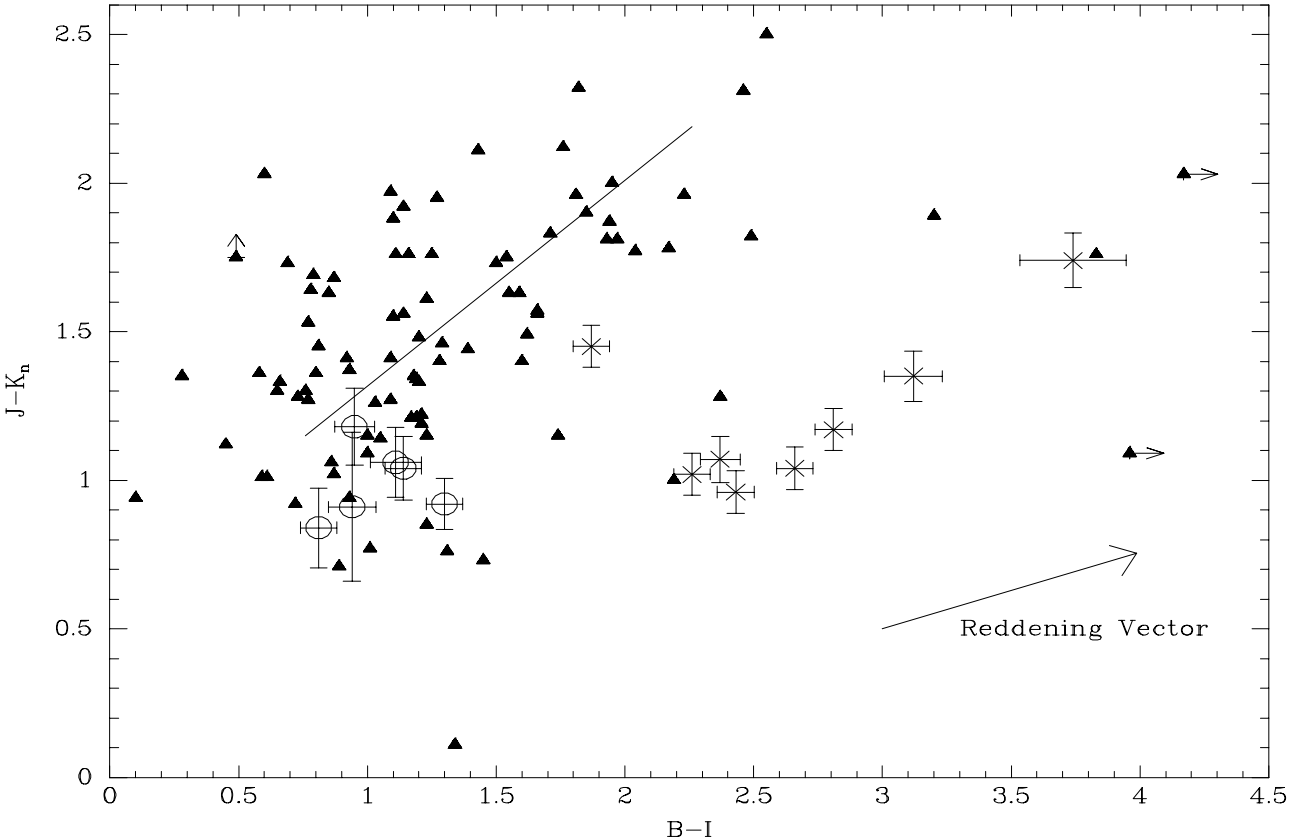


Figure 4—Optical and infrared colours of the complete subset of the Parkes sample (triangles and crosses), compared with a small sample of optically selected LBQS QSOs (circles). Solid triangles denote unresolved sources: crosses are galaxies. The solid line shows where a pure power-law continuum slope would lie: it runs from $F_\nu \propto \nu^0$ on the left end, to $F_\nu \propto \nu^{-2}$ on the right end. Error bars are not shown for the unresolved Parkes sources, but are comparable with those of the optically selected QSOs. The reddening vector is for an extinction $E(B - V) = 0.2$, a redshift of one, and dust extinction as in equation (1). The direction of the reddening vector is independent of redshift.

Our data confirm the basic result of Webster et al. (1995): the Parkes quasars have very different $B - K$ colours from optically selected QSOs (Figure 3). The difference is significant: a Kolmogorov-Smirnov test shows that the probability of getting two samples this different from the same parent population is only 9.1×10^{-5} . The bluest Parkes sources have colours very similar to those of optically selected QSOs, but the distribution of colours extends much further into the red.

3.2 The ‘Main Sequence’

Are the Parkes sources uniformly red everywhere between B and K_n ? In Figure 4 we plot a measure of the optical colour ($B - I$) against a measure of the near-IR colour ($J - K_n$) for the complete sub-sample. Objects whose continuum shape approximates a featureless power-law all the way from B to K_n should lie close to the solid line in this plot.

Approximately 90% of all the Parkes sources do indeed lie close to the power-law line in Figure 4. These sources form a ‘main sequence’ of quasar colours, stretching from blue objects with $F_\nu \propto \nu^{\sim 0}$ to red objects with $F_\nu \propto \nu^{\sim -2}$. Examples of quasars from both ends of this ‘main sequence’ are shown in Figure 5. Note that these quasars can lie on either side of the power-law line: i.e. they can have both ‘n’ and ‘u’ shaped continuum spectra. The majority, however, lie above the line, consistent with slightly ‘u’ shaped spectra (redder in the near-IR than in the optical). This supports the synchrotron model for these sources. We defer discussion of this point to the detailed synchrotron modelling in the companion paper by Whiting, Webster & Francis (2000).

3.3 Optically Selected QSOs

As Figure 4 shows, the optically selected QSOs all have very similar colours, and lie at the blue end of

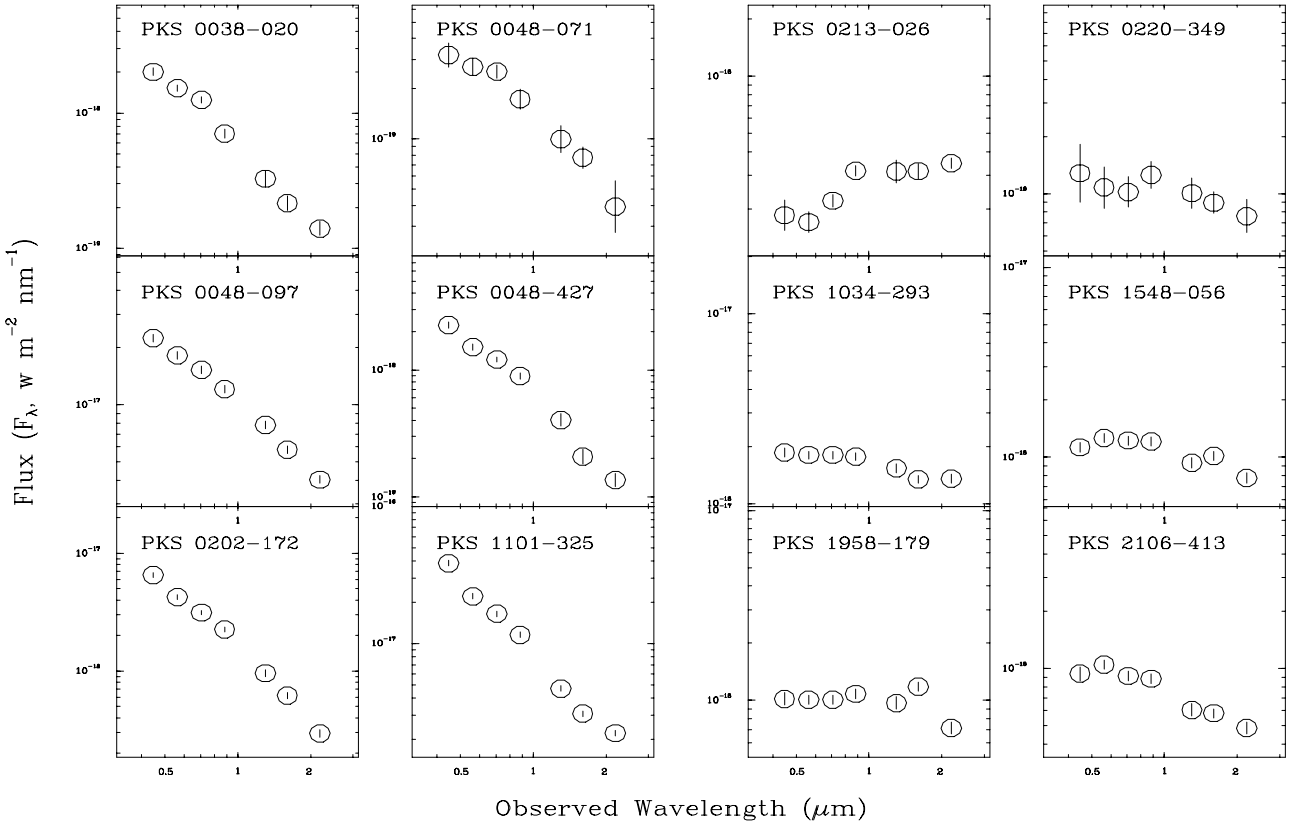


Figure 5—Spectral energy distributions of representative Parkes quasars from the blue (left six plots) and red (right six plots) ends of the ‘main sequence’, as defined in the text. Sources on the left have $J - K_n \leq 1.5$ and $B - I \leq 1.5$; sources on the right have $J - K_n > 1.8$ and $3 > B - I > 1.8$.

the ‘main sequence’. They lie systematically below the power-law line, however, indicating that they have ‘n’ shaped spectra: i.e. they are redder in the optical than in the near-IR. This can be seen in their spectra energy distributions, shown in Figure 6.

This spectral curvature matches the predictions of the dust model. Wills, Netzer & Wills (1985), however, suggested that it may be partially due to blended Fe II and Balmer-line emission, though Francis et al. (1991) argued that this curvature is too large to be plausibly explained by emission-line contributions.

The position of the optically selected QSOs at the blue end of the ‘main sequence’ would be expected if the cause of redness in the Parkes quasars is the addition of a red synchrotron component to an underlying blue continuum which is identical to that in radio-quiet QSOs (Whiting, Webster & Francis 2000).

3.4 Galaxies and Extremely Red Objects

The spectra of the spatially extended sources in the Parkes sample are sharply peaked in the red, as would be expected from moderate redshift galaxies (Figure 7). They therefore lie far below the ‘main sequence’ in Figure 4, the one exception being

PKS 1514–241, which is a galaxy at $z = 0.049$ with a BL Lac nucleus, which is presumably diluting the galaxy colours. Higher redshift galaxies lie further to the right on this plot, as would be expected due to the 400 nm break reducing the B -band flux.

What are the other, red, highly ‘n’ shaped objects lying far below the ‘main sequence’ which are not spatially resolved? A few are high redshift QSOs, in which the B -band flux has been reduced by Ly α forest absorption (Figure 8). The reddest objects, however, with $B - I > 3$ (Figure 9), do not lie at high redshifts. We have obtained spectra of four of these very red objects (Francis et al. 2000, in preparation). Three show hybrid spectra: they look like galaxies at short wavelengths, but at longer wavelengths a red power-law continuum component is seen, along with broad emission lines. The ratios of H α to H β are around 20: far above those seen in normal AGN (~ 5) and evidence of substantial reddening (Figure 10). Note that these hybrid objects all have radio spectra indices near the steep spectrum cut-off of our sample, as do the galaxies in the sample.

The reddest objects are thus a heterogeneous group: some are high redshift quasars, some are galaxies, and some are heavily dust-reddened quasars.

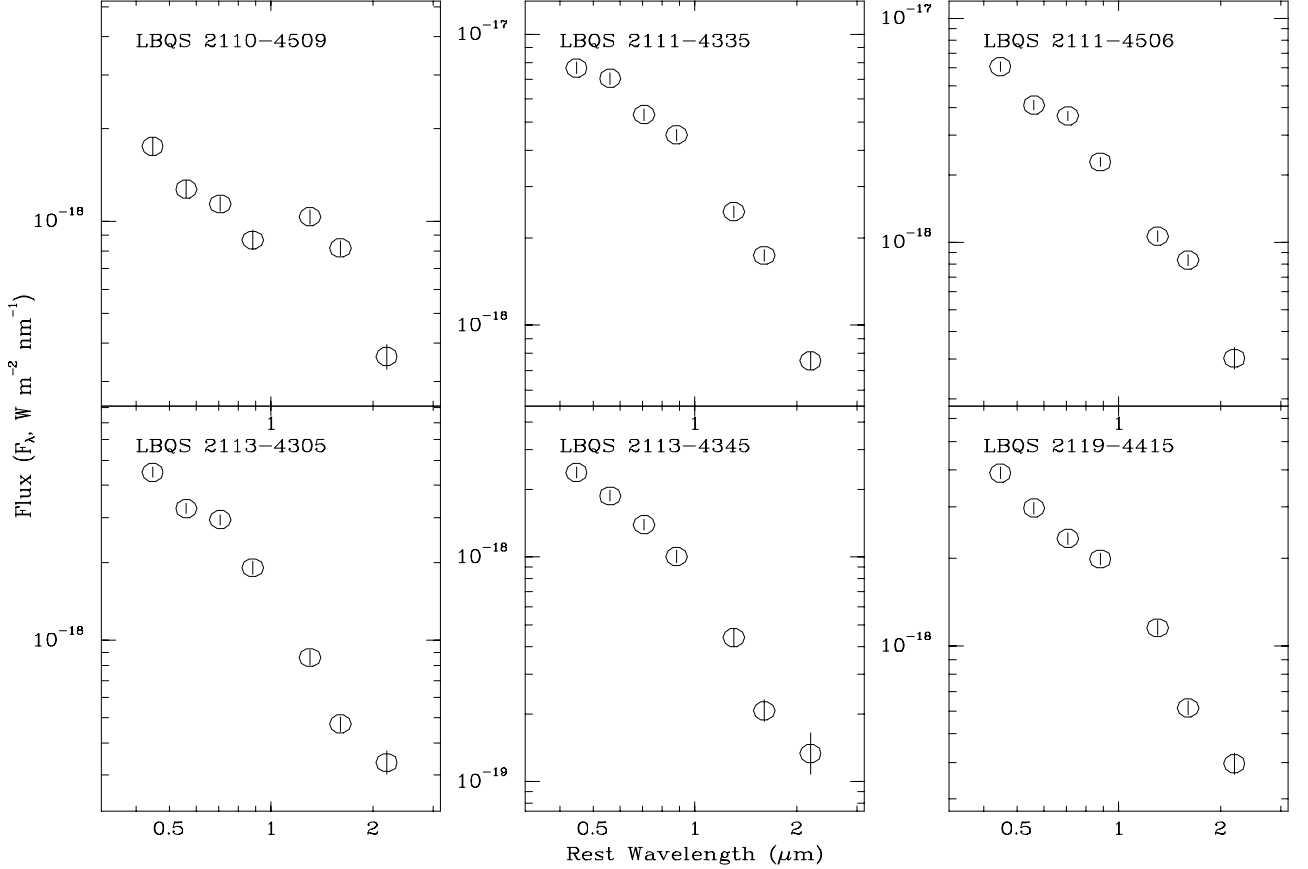


Figure 6—Spectral energy distributions of all six optically selected QSOs with complete photometric data.

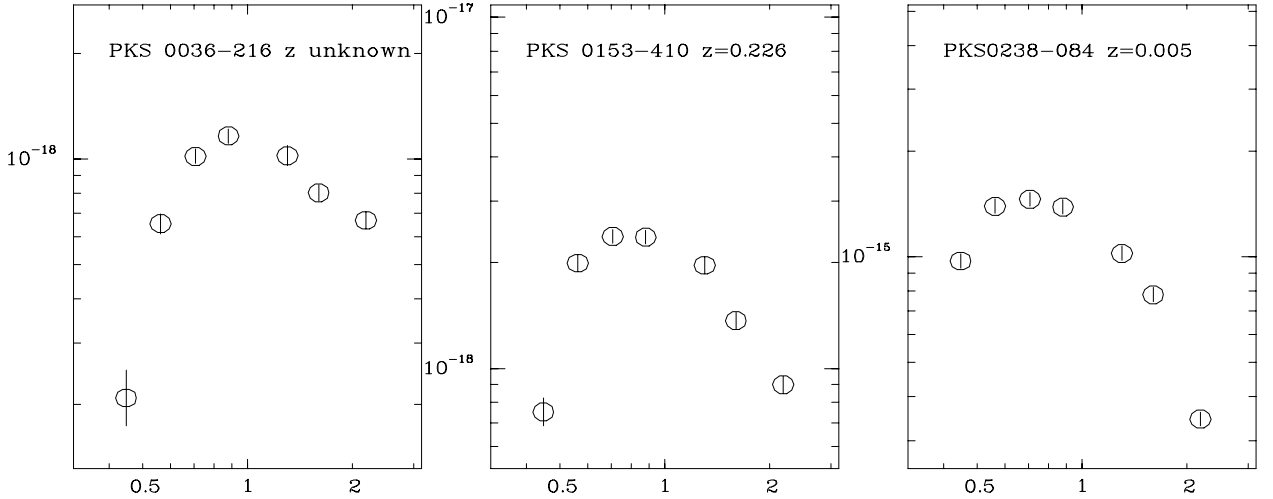


Figure 7—Spectral energy distributions of three representative galaxies from the Parkes sample.

3.5 Unidentified Objects

Four Parkes sources were not detected in any band. After correction for galactic foreground absorption (Schlegel, Finkbeiner & Davis 1998), our non-detections impose 3σ upper limits of $H > 19.61$ for PKS 1532+004, $H > 19.76$ and $K > 19.29$ for PKS 1601-222, $H > 17.22$ and $K > 16.61$ for PKS 1649-062 (which is subjected

to substantial galactic reddening) and $H > 19.82$ for PKS 2047+098.

If unified schemes for radio-loud AGN are correct, the host galaxies of our flat-radio-spectrum sources should be very similar to those of steep-radio-spectrum radio galaxies. This enables us to place a lower-limit on the redshift of these unidentified sources: even if their AGN light is completely obscured, we should still see the host galaxy, which

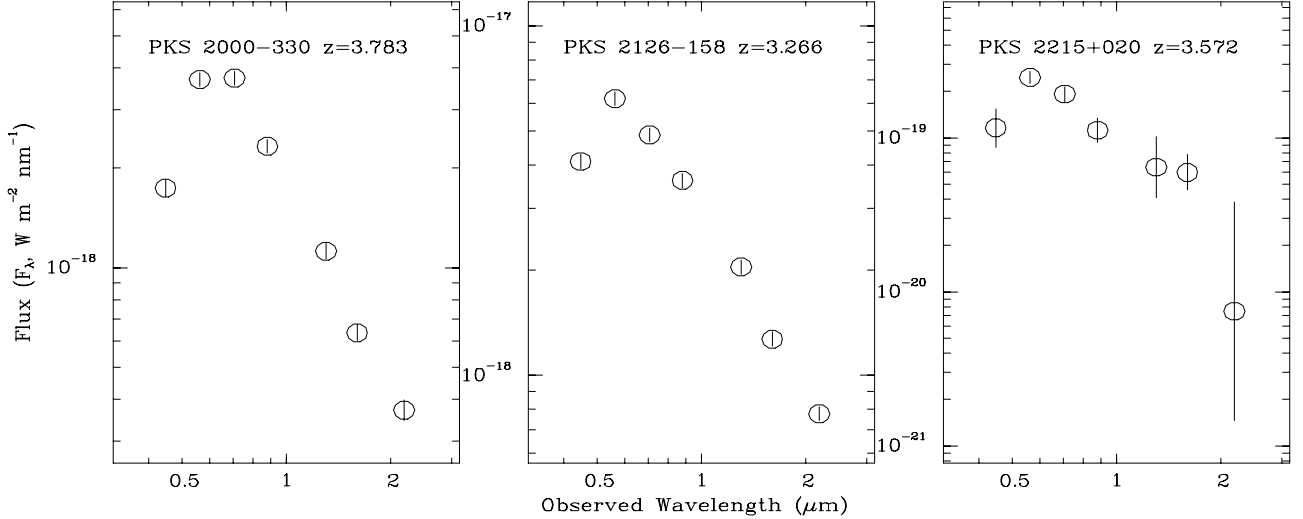


Figure 8—Spectral energy distributions of three representative Parkes quasars with redshifts $z > 3$, showing the dip in the B -band caused by Ly α forest absorption.

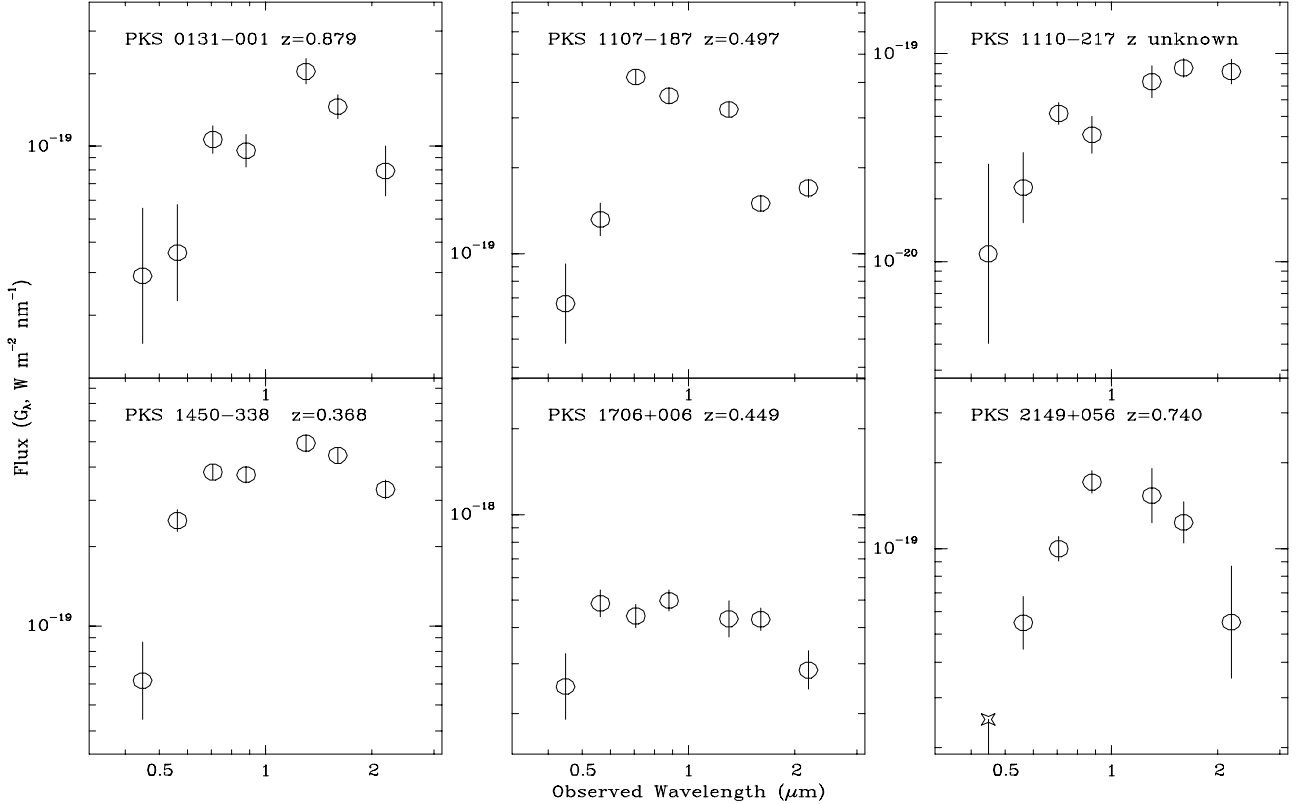


Figure 9—Spectral energy distributions of the six Parkes sources with $B - I > 3$. The data for PKS 1706+006 have been adjusted for galactic dust extinction of $E(B - V) = 0.23$ (Schlegel, Finkbeiner & Davis 1998), assuming a dust extinction law as described in the text.

should lie on the K -band Hubble diagram for radio galaxies (e.g. McCarthy 1992). To be undetected at our magnitude limits, therefore, all these sources must lie above redshift 1, and apart from PKS 1649-062, probably lie above redshift 3.

3.6 Anomalous Objects

Three sources have colours that do not fit any of these categories (Figure 11). We discuss these in turn.

PKS 1648+015 shows a smooth optical power-law rising into the red, until at around $1.4 \mu\text{m}$, the flux abruptly decreases. As all the IR data points were taken within minutes of each other in good weather conditions, we believe that this near-IR turn-over is real. We obtained a somewhat noisy optical spectrum of this source (Drinkwater et al. 1997) which shows a featureless, very red power-law, in excellent agreement with the photometry. We cannot explain this source.

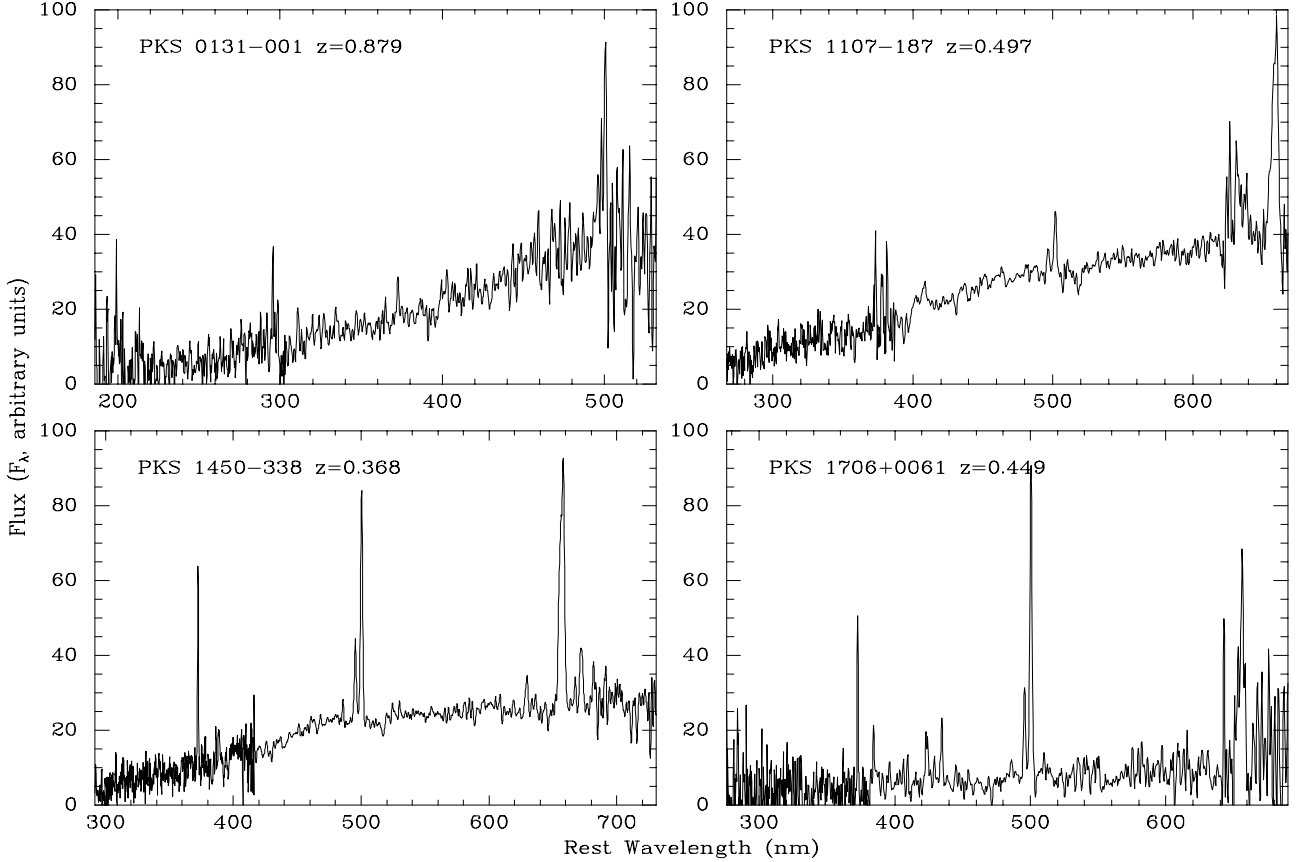


Figure 10—Optical spectra of four extremely red Parkes sources. With the exception of PKS 0131–001, the spectra show features both of galaxy light (the 400 nm break and narrow [O II] 372·7 nm and [O III] 495·9/500·7 lines) and of dust-reddened quasar light (a red continuum at long wavelengths, broad H α 656·3 nm line emission, and the notable weakness of the broad H β 486·1 nm line with respect to H α).

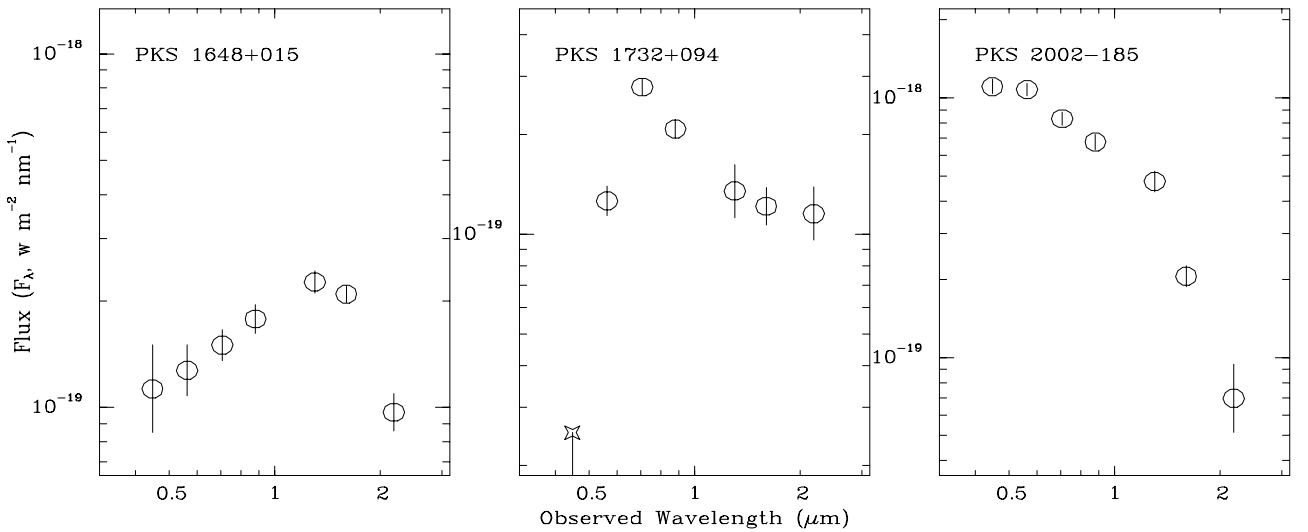


Figure 11—Spectral energy distributions of three anomalous Parkes sources.

PKS 1732+094 is blue longwards of around $0\cdot6\,\mu\text{m}$, but drops dramatically at shorter wavelengths. Our spectrum of this source (Drinkwater et al.) is too poor to be of any use. We hypothesise that this may be a very high redshift $z > 4$ quasar, and that the drop in the blue is due to Ly α absorption.

PKS 2002–185 has optical colours typical of the bluest Parkes sources, but in the near-IR is bluer still: far bluer than any other source at these wavelengths. An optical spectrum, covering a very restricted wavelength range (Wilkes et al. 1983) shows only a single broad emission-line: on the

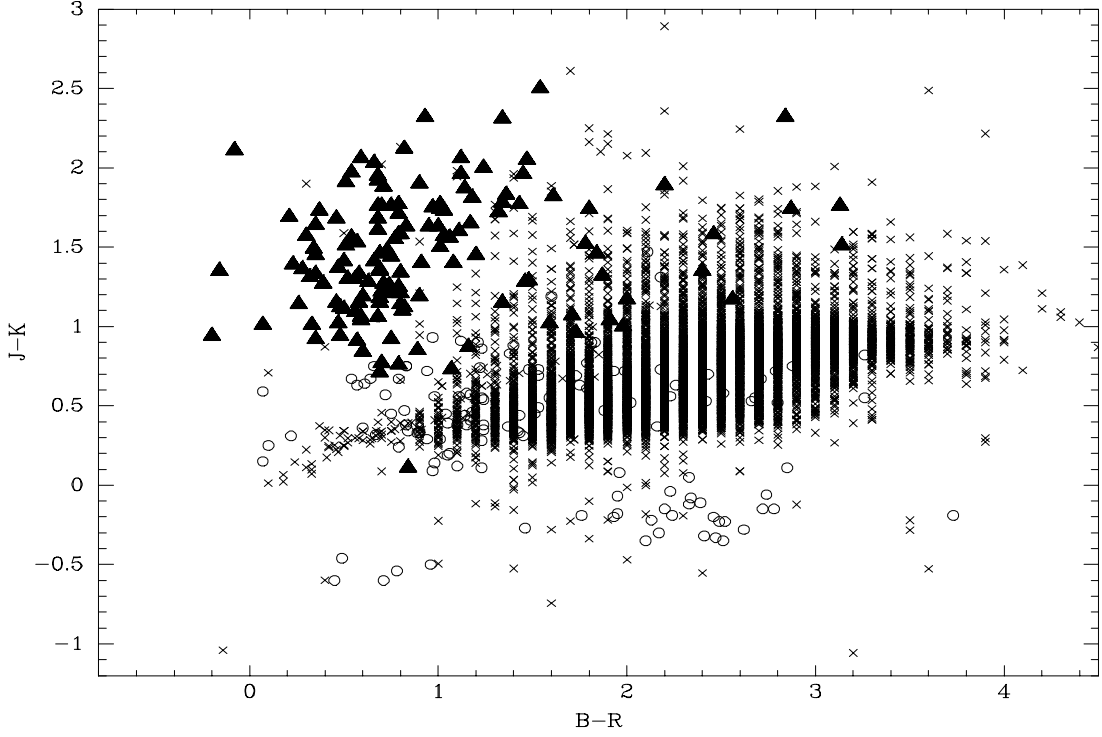


Figure 12—Optical and near-IR colours of the Parkes sources (triangles) compared to photometry of 6400 high galactic latitude point sources drawn from the 2MASS survey (crosses) and sources with $K \leq 22$ from the EIS Hubble Deep Field data release (circles, Benoist et al. 1999).

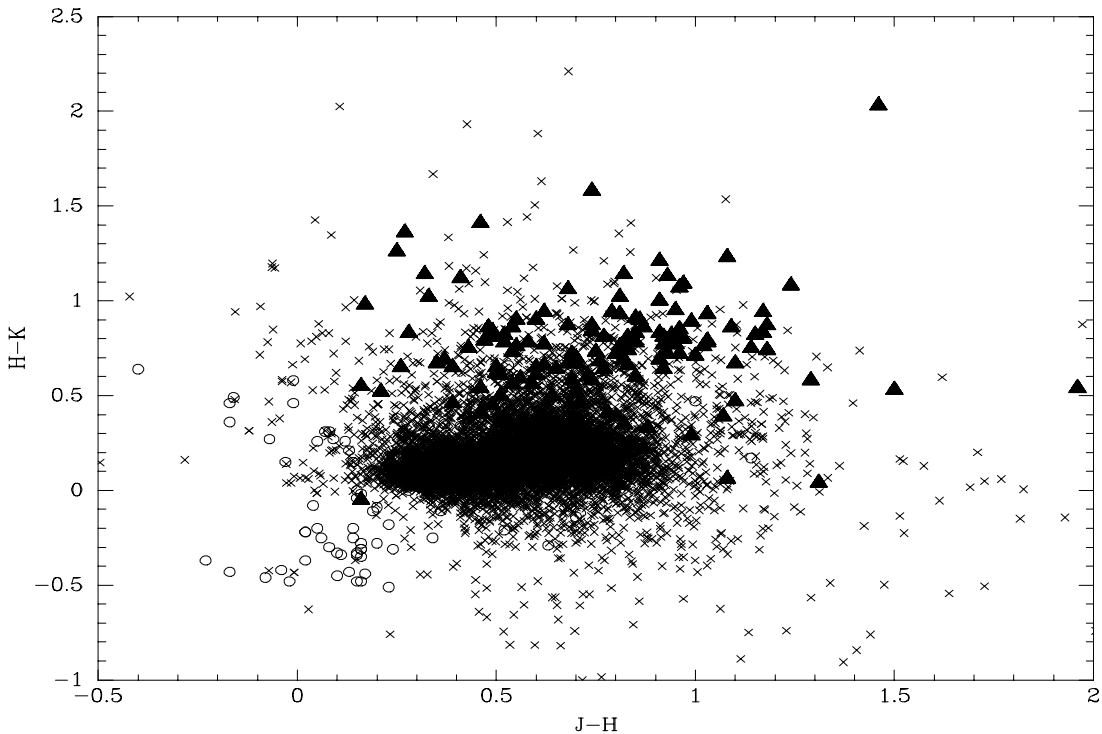


Figure 13—Near-IR colours of the Parkes sources (triangles) compared to photometry of 6400 high galactic latitude point sources drawn from the 2MASS survey (crosses) and sources with $K \leq 22$ from the EIS Hubble Deep Field data release (circles, Benoist et al. 1999).

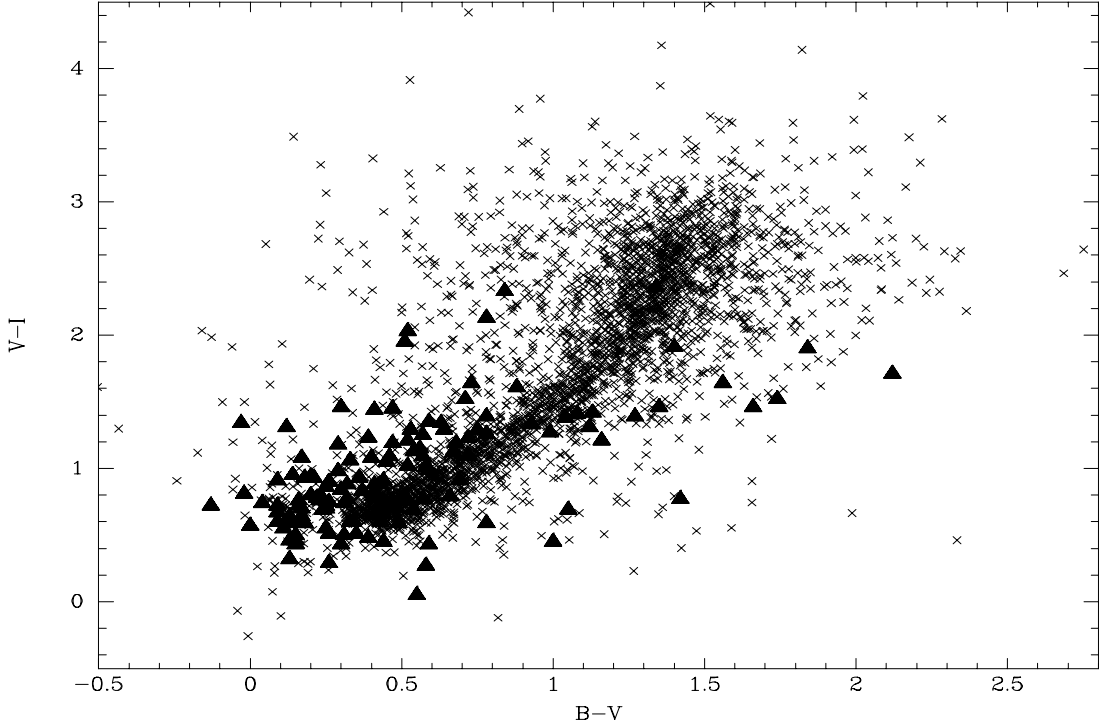


Figure 14—Optical colours of the Parkes sources (triangles) compared to photometry of 3200 high galactic latitude point sources drawn from the EIS wide survey (crosses, Prandoni et al. 1999).

assumption that this is Mg II (279.8 nm) a redshift of 0.859 is determined.

4 Multicolour Selection of Red Quasars

Could there be a population of radio-quiet QSOs with the same colours as our radio-loud red quasars? Webster et al. (1995) showed that it is virtually impossible to find such QSOs in any sample with a blue optical magnitude limit. In this section we ask whether red QSOs could be identified by colour selection in the red optical and near-IR.

In Figure 12, we compare the optical and near-IR colours of the Parkes sources against the colours of high galactic latitude point sources drawn from the Two-Micron All Sky Survey (2MASS, $K \leq 15$) and the ESO Imaging Survey (EIS, $K \leq 22$). The ‘Main Sequence’ sources, both red and blue, are clearly separated from the foreground objects. This separation is due to their power-law spectral energy distributions: as compared to the convex spectral energy distributions of stars and galaxies, the quasars have excess flux in B and/or K . This selection technique is similar to the ‘KX’ technique proposed by Warren, Hewett & Foltz (2000). Unfortunately, the very red sources lying below the ‘main sequence’ have colours within the stellar locus and will be hard to find.

Can red quasars be identified purely on the basis of their near-IR colours? In Figure 13, we show that most of the Parkes quasars lie in regions of the near-IR colour–colour plot with substantial stellar contamination, but that the reddest move away

from the stellar locus, and could be detectable in the IR alone. Figure 14 shows that purely optical colour selection is not likely to be effective.

5 Conclusions

The Parkes quasars can, we conclude, be crudely divided into three populations:

- (1) **The ‘Main Sequence’:** About 90% of the Parkes sources have approximately power-law spectral energy distributions, with spectral indices α ($F_\nu \propto \nu^\alpha$) in the range $0 > \alpha > -2$. The nature of these sources is discussed by Whiting, Webster & Francis (2000).
- (2) **Very Red Sources:** These sources, which comprise $\sim 10\%$ of the Parkes sample, are characterised by much redder continuum slopes in the optical than in the IR. They tend to have relatively steep radio spectra. Half these sources are radio galaxies, while most of the remainder are highly dust-reddened quasars. The undetected sources are probably high redshift members of this class.
- (3) **Oddballs:** Roughly 2% of the Parkes sample defy this categorisation.

The ‘main sequence’ sources, both red and blue, should be easily detectable in combined near-IR and optical QSO surveys, due to their excess flux in the K and/or B bands.

Acknowledgments

We wish to thank Mike Bessell and Peter McGregor for their help with the details of the photometry, and Tori Ibbetson for her assistance with the observations. This publication makes use of data products from the Two Micron All Sky Survey, which is a joint project of the University of Massachusetts and the Infrared Processing and Analysis Center, funded by the National Aeronautics and Space Administration and the National Science Foundation, and of catalogues from the ESO Imaging Survey, obtained from observations with the ESO New Technology Telescope at the La Silla observatory under program-ID Nos 59.A-9005(A) and 60.A-9005(A).

References

- Benoist, C., et al. 1999, *A&A*, 346, 58
 Bersanelli, M., Bouchet, P., & Falomo, R. 1991, *A&A*, 252, 854
 Bessell, M. S., Castelli, F., & Plez, B. 1998, *A&A*, 333, 231
 Carter, B. S., & Meadows, V. S. 1995, *MNRAS*, 276, 734
 Drinkwater, M. J., Webster, R. L., Francis, P. J., Condon, J. J., Ellison, S. L., Jauncey, D. L., Lovell, J., Peterson, B. A., & Savage, A. 1997, *MNRAS*, 284, 85
 Francis, P. J. 1996, *PASA*, 13, 212
 Francis, P. J., Hewett, P. C., Foltz, C. B., & Chaffee, C. B. 1991, *ApJ*, 373, 465
 Graham, J. A. 1982, *PASP*, 94, 265
 Heidt, J., & Wagner, S. J. 1996, *A&A*, 305, 42
 Ledden, S. E., & O'Dell, S. L. 1983, *ApJ*, 270, 434
 McCarthy, P. 1992, *ARA&A*, 31, 639
 McGregor, P., Hart, J., Downing, M., Hoadley, D., & Bloxham, G. 1994, in *Infrared Astronomy with Arrays: The Next Generation*, ed. I. S. McLean (Dordrecht: Kluwer), p. 299
 MacKenty, J. W., et al. 1997, *NICMOS Instrument Handbook, Version 2.0* (Baltimore: STScI)
 Masci, F. J., Webster, R. L., & Francis, P. J. 1998, *MNRAS*, 301, 975
 Morris, S. L., Weymann, R. J., Anderson, S. F., Hewett, P. C., Foltz, C. B., Chaffee, F. H., & Francis, P. J. 1991, *AJ*, 102, 1627
 Neugebauer, G., Green, R. F., Matthews, K., Schmidt, M., Soifer, B. T., & Bennet, J. 1987, *ApJS*, 63, 615
 Prandoni, I., et al. 1999, *A&A*, 345, 448
 Rieke, G. H., Lebofsky, M. J., & Wisniewski, W. A. 1982, *ApJ*, 263, 73
 Schlegel, D. J., Finkbeiner, D. P., & Davis, M. 1998, *ApJ*, 500, 525
 Serjeant, S., & Rawlings, S. 1997, *Nature*, 379, 304
 Stickel, M., Rieke, G. H., Kühr, H., & Rieke, M. J. 1996, *ApJ*, 468, 556
 Wagner, S. J., Sanchez-Pons, F., Quirrenbach, A., & Witzel, A. 1990, *A&A*, 235, L1
 Warren, S. J., Hewett, P. C., & Foltz, C. B. 2000, *MNRAS*, 312, 827
 Webster, R. L., Francis, P. J., Peterson, B. A., Drinkwater, M. J., & Masci, F. J. 1995, *Nature*, 375, 469
 Whiting, M. T., Webster, R. L., & Francis, P. J. 2000, *MNRAS*, submitted
 Wilkes, B. J., Wright, A. E., Jauncey, D. L., & Peterson, B. A. 1983, *PASA*, 5, 2
 Wills, B., Netzer, H., & Wills, D. 1985, *ApJ*, 288, 94